Magnetic excitations in the weak itinerant ferromagnet MnSi

Y. Ishikawa,* G. Shirane, and J. A. Tarvin
Brookhaven National Laboratory,† *Upton, New York 11973*

M. Kohgi
Physics Department, Tohoku University, Sendai, Japan
(Received 12 August 1977)

Magnetic excitations in an intermetallic compound MnSi have been studied by neutron scattering. At 5 K in a magnetic field of 10 kOe, well-defined spin-wave excitations have been observed below 2.5 meV. The dispersion relation is almost isotropic and is $\hbar\omega_q(\text{meV}) = 0.13 + 52q^2$ (Å^{-2}) in the [100] direction. Above 3 meV, the excitation linewidth increases substantially, suggesting that the dispersion relation merges into the Stoner continuum. The Stoner excitations, which extend over almost all of the Brillouin zone, show a broad peak on the extension of the spin-wave dispersion relation. The spin-wave excitation renormalizes with increasing temperature and collapses into critical scattering above 40 K. On the other hand, the excitation in the Stoner continuum is affected little by temperature; the excitations are qualitatively the same at $T/T_N = 10$ as at 5 K. The Stoner boundary energy decreases with increasing temperature. The results provide us with the first example of magnetic excitations in a weak itinerant ferromagnet.

I. INTRODUCTION

The cubic transition-metal monosilicides *M*Si ($M =$ Mn, Fe, Co) with the *B*20 structure have attracted the attention of a number of investigators because of their varieties in both magnetic and electric properties[1-3]: MnSi is metallic and it behaves ferromagnetically in a magnetic field,[1-4] while FeSi and CoSi, being semimetallic,[5] have paramagnetic[6,7] and diamagnetic[1,2] properties, respectively. A weak ferromagnetism appears in the solid solution between FeSi and CoSi.[3] The compounds are now considered to provide a typical example of the *d*-band magnetism with a relatively weak correlation just as $ZrZn_2$.[8]

A recent neutron small-angle diffraction study has revealed that in zero field MnSi has the helical spin structure below 29.5 ± 0.5 K with a long period of 180 Å propagating along the [111] direction.[9] In a magnetic field greater than 6 kOe, however, the crystal is saturated with a spontaneous magnetic moment of 0.4 μ_B, which is substantially smaller than the effective moment of 1.4 μ_B evaluated from the Curie-Weiss relation in the paramagnetic region.[4] The magnetization at 0 K still increases even in a magnetic field of 150 kOe and shows a strong volume dependence.[10] The magnetization in a magnetic field $M(H,T)$ decreases with temperature T just as the classical band theory for weak itinerant ferromagnetism predicts[11,12]

$$\left(\frac{M(H,T)}{M(0,0)}\right)^2 - \frac{2\chi_0 H}{M(H,T)} = 1 - \left(\frac{T}{T_c}\right)^2 . \qquad (1)$$

The entropy associated with the magnetic ordering estimated from the anomaly of the specific heat at the critical temperature is an order of magnitude smaller than that expected for the localized spin system.[13] The nuclear-spin relaxation time in the paramagnetic region is independent of temperature, but with the values two orders of magnitude smaller than the case where the localized spin of 1.4 μ_B exists.[11]

All these facts suggest that MnSi in the induced ferromagnetic (paramagnetic) state can be classified as a weak itinerant ferromagnet. The magnetic phase diagram of MnSi determined by an ultrasonic method is reproduced in Fig. 1.[14,15] A solid line in the figure represents the phase boundary where the helical component of the magnetic moment $\langle S_Q \rangle$ disappears, while a broken line indicates a boundary where the magnetic moment induced in the field direction $\langle S_0 \rangle$ decreases distinctly.[15] The ultrasonic attenuation has a broad maximum there.[14]

This paper describes the magnetic excitations in MnSi observed by inelastic neutron scattering. The main purpose of the investigation is to find out the magnetic excitations typical of the weak itinerant ferromagnet.[16] There has been a long debate on the electronic state of magnetic carriers in the transition metals and alloys.[17] The measurement of the magnetic excitations in these materials by means of neutron scattering is the most direct method to settle this question, because the dynamical response of the itinerant electron to the magnetic field should be quite different from that of the localized spin system (Heisenberg system); in the case of the itinerant elec-

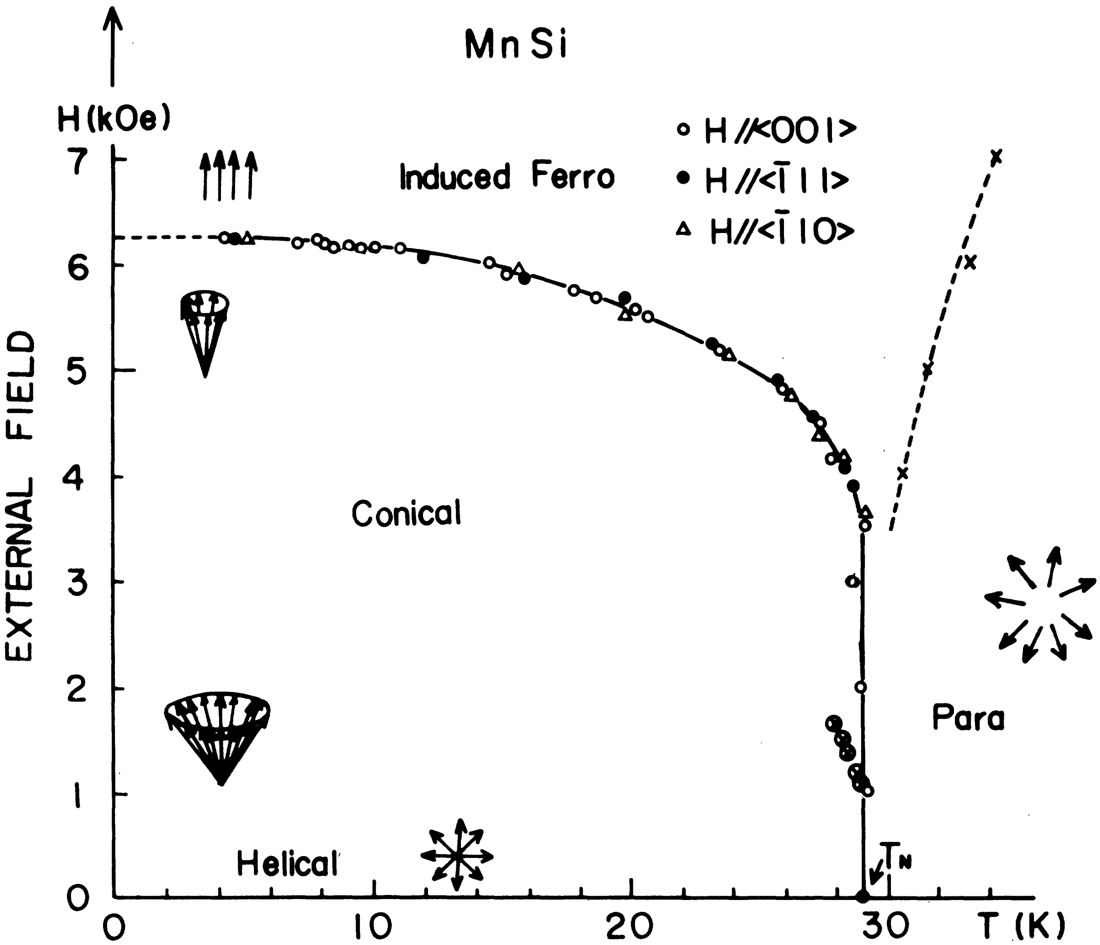

FIG. 1. Magnetic phase diagram of MnSi.

tron ferromagnet, the single-particle excitation called Stoner excitation should exist in addition to the collective spin-wave excitation as schematically illustrated in Fig. 2. However, the experimental studies of the spin dynamics in the metallic ferromagnets are quite limited[16] and only a few experimental results have provided clear evidence for the itinerant character of magnetic carriers.[18] The Oak Ridge group found that the intensity of neutron spin wave scattering in ferromagnetic nickel[19] and iron[20] decreases substantially when the spin-wave energy exceeds 100 meV. The phenomenon has been interpreted as indicating the existence of Stoner excitations beyond 100 meV, but the Stoner excitations themselves have never been observed in the ferromagnetic state because of experimental difficulties.

The weak itinerant electron ferromagnet is the most promising system to explore this problem, because the Stoner splitting Δ of the d band is expected to be sufficiently small and the Stoner excitation should oc-

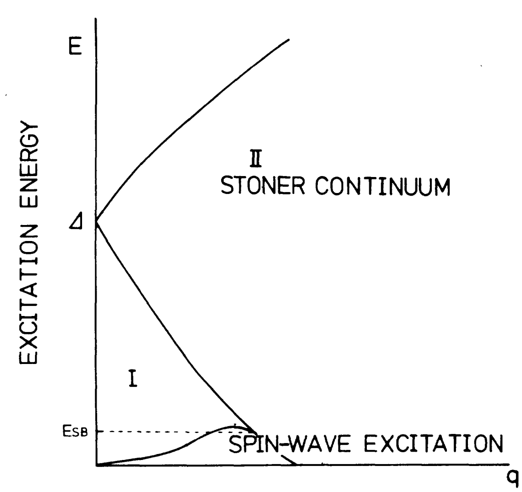

FIG. 2. Schematical plot of magnetic excitation in a ferromagnetic electron gas expected by RPA theory.

cur in a relatively low-energy region. Furthermore Moriya and Kawabata developed a band theory (MK theory) which takes into account the transverse spin fluctuation in a self-consistent way and showed that the long-wavelength spin fluctuations play the most important role in determining the temperature dependence of magnetic properties of the weak itinerant ferromagnet.[21] Therefore, the observation of the magnetic excitations in this system would give not only information on the chartacteristic spin dynamics of the weakly ferromagnetic itinerant electron system, but also an experimental test of the MK theory. The results would also give an insight to the dynamical response of the strongly ferromagnetic transition metals.

The format of this paper is as follows. In Sec. II we describe the sample characterization as well as experimental techniques. The experimental results at 5 K and higher temperatures are presented in Sec. III and are discussed based on the random-phase approximation (RPA) for the electron gas in Sec. IV.

II. EXPERIMENTAL DETAILS

A. Crystal and crystal structure

The crystal was grown from the melt by Czochralski method at the Institute for Iron Steel and Other Metals, Tohoku University. A cylindrical crystal 20 mm in diameter and 40 mm in length with the $[01\bar{1}]$ long axis was used in the experiment. The crystal has a mosaic spread of less than 15 min. Parts of the crystal have been used for other kinds of experiments such as ultrasonic attenuation,[14] ESR,[22] and neutron small-angle diffraction[9]; the crystal has, therefore, been characterized well. MnSi has the cubic $B20$-type crystal structure[23] with the space group $P2_13(T^4)$ and with a unit cell containing four manganese atoms in the positions $(u,u,u;\frac{1}{2}+u,\frac{1}{2}-u,\bar{u};\frac{1}{2}-u,\bar{u},\frac{1}{2}+u;\bar{u},\frac{1}{2}+u,\frac{1}{2}-u)$ and four silicon atoms in a similar set. The positional parameters u_{Mn} and u_{Si} are given in Table I. In this structure, manganese and silicon atoms are displaced in opposite $\langle 111 \rangle$ directions from the fcc position. Each manganese atom has six nearest-neighbor (nn) manganese atoms at the equidistance of 2.795 Å, while it is surrounded by seven silicon atoms, one at 2.305 Å in a $\langle 111 \rangle$ direction, three at 2.701 Å, and another three at 2.836 Å. Note that the nn Mn-Mn distance is almost the same as that in γ manganese metal (2.725 Å).

The nuclear and magnetic structure factors $|F(hkl)|^2$ for neutron diffraction were calculated and are tabulated in Table I. For the magnetic structure factors, the ferromagnetic state with the magnetic moment of 0.4 μ_B only in the manganese site was assumed and the magnetic form factor of Mn^{2+} ion was adopted. Note that, because of noncubic point symmetry of each site, the structure factor of the reflections with mixed indices are not necessarily invariant for the change of order of indices (h,k,l) [for example, $F(210) \neq F(201)$]. Table I gives information not only on the intensities of nuclear and magnetic Bragg reflections, but also on the intensities for inelastic scattering of the acoustical-phonon and magnon modes; i.e., the magnon scattering should be studied in the Brillouin zones around the (110), (111), or (210) reciprocal-lattice points; the last one is the best because of the small structure factor for phonon scattering. This was used to distinguish magnon scattering from phonon scattering as will be described in Sec. II B.

TABLE I. Nuclear (F_N^2) and magnetic (F_M^2) structure factors of MnSi at 0 K. F_M^2 includes the magnetic form factor. $a = 4.558$ Å, $u_{\mathrm{Mn}} = 0.138$, $u_{\mathrm{Si}} = 0.845$, $M = 0.4\mu_B$.

h	k	l	F_N^2	F_M^2
1	0	0	0	0
0	1	1	2.362	0.0269
1	1	1	2.624	0.0230
2	0	0	0.143	0.0015
2	0	1	3.479	0.0225
0	2	2	0.036	0.0000
3	0	0	0	0
1	2	2	0.308	0.0005
2	2	2	8.016	0.0122

B. Instrumental

The experiments were carried out with a neutron triple-axis spectrometer at the Brookhaven High Flux Beam Reactor. Pyrolytic graphite reflecting from the (002) plane was used for both monochrometer and analyzer. Most of the measurements were performed with fixed outgoing neutron energy of either 14.8 ($14.8E_f$) or 24 meV ($24E_f$). Horizontal collimators of 40′-20′-40′-40′ were used unless otherwise mentioned. When higher resolution was required for small energy transfers, the scans were also made with fixed incoming neutron energy of 14.8 meV ($14.8E_i$) and with collimators of 20′-20′-20′-40′. In both cases of $14.8E_f$ and $14.8E_i$, 5-cm pyrolytic graphite filters were inserted in the neutron path to remove higher-order contamination.

The neutron magnetic cross section from a cubic system is given for unpolarized neutrons by[24]

$$\frac{d^2\sigma}{d\Omega\, d\omega} = \left(\frac{\gamma e^2}{mc^2}\right)^2 \frac{k_f}{k_i} |f_m(Q)|^2 \times \Sigma^\alpha (1 - e_q^{\alpha 2}) S^{\alpha\alpha}(Q,\omega) \quad , \tag{2}$$

with conventional notation. The scattering function $S^{\alpha\beta}(Q,\omega)$ is given, in general, by the imaginary part of the generalized spin susceptibility[24]

$$S^{\alpha\beta}(Q,\omega)=\frac{1}{\pi N}\frac{\hbar}{1-e^{-\hbar\omega/kT}}\operatorname{Im}\chi^{\alpha\beta}(Q,\omega) \quad . \tag{3}$$

The measured intensity $I(Q,\omega)$ is given by the convolution of the cross section with a resolution function of the spectrometer $R(\Delta Q,\Delta\omega)$;

$$I(Q,\omega)=\int\frac{d^2\sigma}{d\omega\, d\Omega}(Q',\omega') \times R(Q-Q',\omega-\omega')\,d\omega'\,dQ' \quad . \tag{4}$$

In analyzing the intensities obtained from neutron-scattering experiments, care has to be taken with respect to resolution effects, together with possible changes in the analyzer reflectivity. In a constant E_f scan, the analyzer reflectivity is constant, and the $1/k_i$ term in Eq. (2) is cancelled by the $1/k_i$ efficiency of the neutron monitor since the data were taken at constant monitor counts. Therefore ideally the measured intensity is directly proportional to $S(Q,\omega)$, if the resolution correction is carried out. In practice, however, the monitor counts neutrons with higher-order contaminations. This correction has not been performed in this experiment, but the effects have been estimated to be less than 10% for an incident neutron energy higher than 28 meV.[25]

Where the magnetic excitations are sharp, the Gaussian form of the resolution function given by Cooper and Nathans[26] was used for $R(\Delta Q,\Delta\omega)$ in Eq. (4) to estimate the observed linewidths of inelastic peaks.

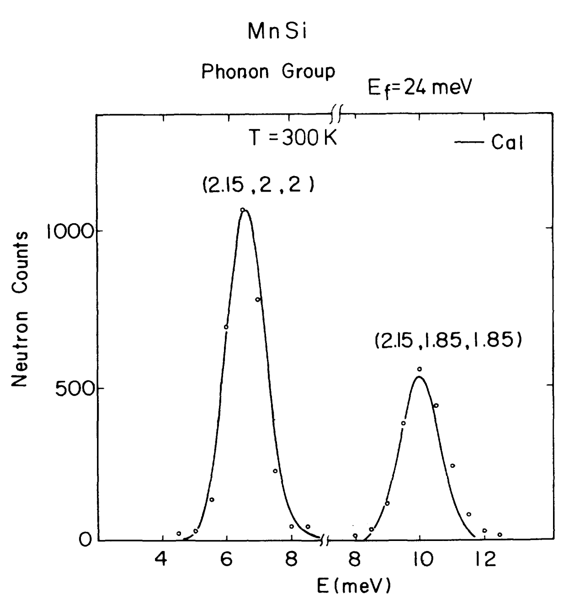

FIG. 3. Scattering profiles calculated by Eq. (4) and typical fits to phonon data.

The profiles of phonon groups calculated for phonons with infinite lifetime agree satisfactorily with observations as displayed in Fig. 3, indicating that the instrumental parameters used in the calculation were correct. The resolution correction to the observed intensity has been investigated in detail by several authors.[26,27] They showed that the measured integrated intensity I of a sharp excitation spectrum is proportional to the scattering function $S(\overline{Q},\overline{\omega})$ at the center of scans $(\overline{Q},\overline{\omega})$; $I=AS(\overline{Q},\overline{\omega})$ with a constant A depending on the experimental condition. Therefore, the intensities of sharp excitations measured in different conditions can be compared by measuring the ratio of the constant prefactors. Where the excitations are relatively broad and smooth, the scattered intensity is directly proportional to $S(Q,\omega)$ for a constant E_f scan and no resolution correction is necessary.

III. EXPERIMENTAL RESULTS

A. Low-energy excitation in a magnetic field of 10 kOe

The crystal with a vertical $[01\bar{1}]$ axis was mounted in a variable temperature cryostat inserted in a superconducting magnet and most of the data were collected around the (011) reciprocal point in a $(01\bar{1})$ zone with a magnetic field of 10 kOe applied in the $[01\bar{1}]$ direction. Some observations were also made around the (210) and (201) reciprocal-lattice points to distinguish magnon scattering from phonon scattering. The crystal was then oriented with a [100] vertical axis. Figure 4 shows an example of neutron groups detected at 5 K along the [100] axis using constant Q mode of operation and $14.8E_f$ in a magnetic field of 10 kOe. Figure 4 indicates that a well-defined spin-wave excitation exists below a momentum transfer of $\zeta=0.17$ ($q=0.234\,\text{Å}^{-1}$). Arrows in each neutron group indicate the full width at half-maximum (FWHM) of the spectrum calculated by Eq. (4) for the magnon with infinite lifetime. This represents the instrumental resolution. The results suggest that the observed magnon groups have small intrinsic linewidth.

When the wave vector exceeds $\zeta=0.18$, however, the linewidth of neutron groups develops discontinuously as displayed in the upper two diagrams of Fig. 4. Neutron groups with energy transfers higher than 4 meV could not be detected with the condition of $14.8E_f$. Similar results were also obtained for the [011] and [111] directions. The spin-wave energies determined in three directions are plotted against the square of the wave vector in Fig. 5. The data have been corrected for resolution effects; when the spin-wave energy has lower than 1.5 meV, the peak position of the observed neutron group was shifted to the higher-energy side by about 0.06 meV with respect to

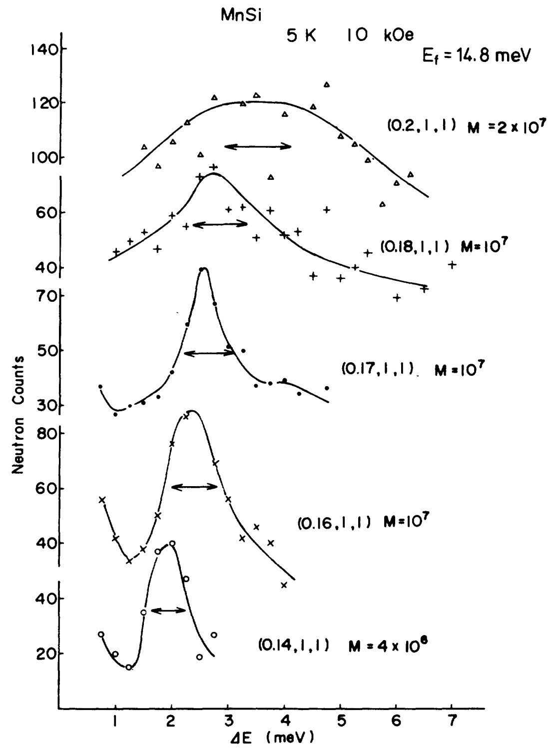

FIG. 4. Magnon groups observed at 5 K in a field of 10 kOe in the [100] direction around (011) with constant Q mode of operation using $E_f = 14.8$ meV. M is monitor counts ($10^7 = 7.5$ min). Solid line is smooth connection of experimental data, arrows indicate the FWHM of spectra calculated by Eq. (4) for magnons with infinite lifetime.

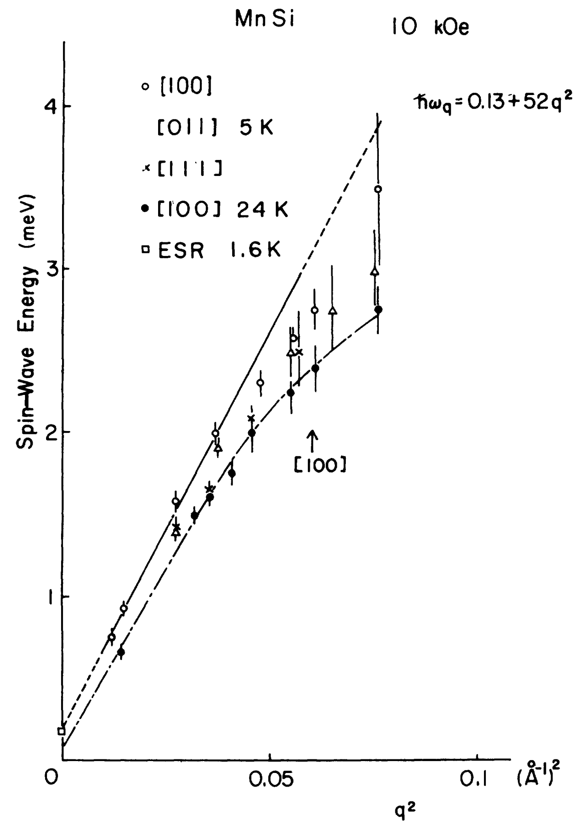

FIG. 5. Spin-wave dispersion in three directions determined at 5 and 24 K. Solid line represents a relation $\hbar\omega_q = 0.13 + 52q^2$.

the dispersion surface, but the resolution correction was not important for higher-energy transfers. As seen in Fig. 5, the dispersion is almost isotropic and a quadratic relation holds only below 2 meV. The dispersion in the higher-energy region deviates from the quadratic relation toward the low-energy side. The spin-wave excitation extrapolated to zero wave vector is 0.13 ± 0.02 meV which agrees satisfactorily with the ESR frequency in a field of 10 kOe measured at 1.6 K for the specimen of the same origin.[22] The dispersions with a quadratic relation are given by

$$\hbar\omega_q(\text{meV}) = 0.13 \pm 0.02 + (50 \pm 2)q^2(A^{-2}) \quad \text{for [100]} ,$$

$$\hbar\omega_q(\text{meV}) = 0.13 \pm 0.02 + (46 \pm 4)q^2(A^{-2}) \quad \text{for [011] and [111]} . \tag{5}$$

An example of the temperature dependence of the spin-wave excitation is shown in Fig. 6(a). The neutron groups in Fig. 6(a) were measured around the center of the reciprocal place (000) with $14.8E_i$ and with collimators of 20′-20′-20′-40′. A chain line in Fig. 6(a) is the instrumental resolution of the spin wave with this energy calculated by Eq. (4). The spin-wave excitation renormalizes with temperature but a well-defined spin-wave group was observed even at 25 K ($T/T_N = 0.85$) for $q = (0.124, 0, 0)$ Å^{-1}. The intrinsic linewidth is still almost absent. Above 25 K, critical scattering develops and the collective excitation was hardly observed at 30 K because of the instrumental resolution. This behavior confirms that the scattering is magnetic in origin. The dispersion relation determined at 24 K is also plotted against q^2 in Fig. 5. The temperature dependence of the spin-wave energy at constant wave vector is displayed in Fig. 7 for different wave vectors. For ζ smaller than $\zeta = 0.14$, the temperature dependence corresponds to that of the exchange stiffness constant $D(T)$. Plotted in Fig. 7 also is (broken line) the temperature variation of magnetization at 10 kOe measured for the same crystal to compare with the temperature variation of $D(T)$. The induced ferromagnetic moment decreases with temperature as if it has a Cruie temperature T_C

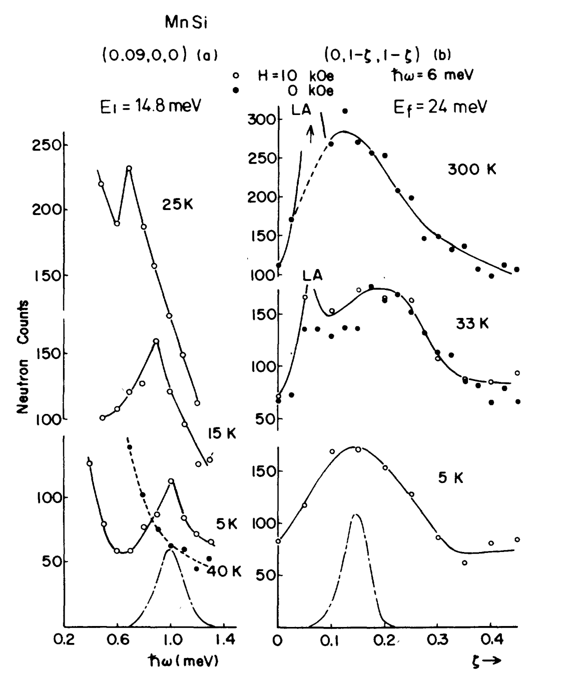

FIG. 6. (a) Magnon groups detected with constant Q mode around (000) using high resolution of 14.8-meV E_i and collimations of 20'-20'-20'-40' at different temperatures. (b) Magnon groups with $E = 6$ meV detected around (011) using $E_f = 24$ meV. Chain lines are calculated by Eq. (4) and represent instrumental resolution.

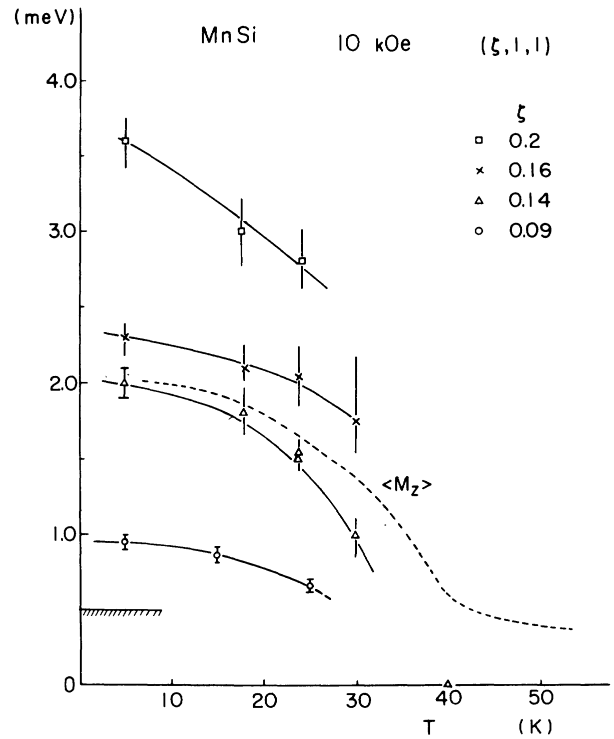

FIG. 7. Temperature variations of spin-wave energy at constant wave vector. The broken line is the magnetization in a field of 10 kOe plotted on an arbitrary scale against temperature. Horizontal line with hatch indicates resolution limit of measurements.

of about 40 K, and $D(T)$ also tends to disappear at this temperature. The temperature dependence thus observed is qualitatively quite similar to the spin dynamics in the Heisenberg system.[24]

B. High-energy excitation at 5 K in a field of 10 kOe

The magnetic excitations above 3 meV were studied with the lower-resolution condition of $24E_f$. When scans were made in the constant E mode of operation, the neutron groups extending over the whole Brillouin zone were detected at 5 K. The neutron group with energy transfer of 6 meV measured in a field of 10 kOe is displayed in Fig. 6(b) as an example. The scattering is distinctly much broader than the instrumental resolution which is also shown by a chain line in Fig. 6(b). Furthermore, what is quite different from the low-energy excitation is that the scattering profile changed very little even if the temperature was raised above the Néel temperature and significant scattering could be detected at 300 K, as shown in the upper diagrams. The profile was also not modified by removing the external field. In order to confirm that this scattering is really magnetic in origin, scans with constant energy transfer at 6 meV were also made at 290 K along both the $(\zeta,0,0)$ and $(\zeta,1,1)$ directions across the Brillouin zones. In case of $(\zeta,1,1)$ scans, broad scattering was detected on both sides of the (011), (111), and (211) reciprocal-lattice points, together with the acoustical-phonon scattering. This is consistent with the fact that the structure factor for magnetic inelastic scattering should be large in these Brillouin zones (cf. Table I). The intensity ratios of the magnetic scattering in different zones are also consistent with the structure factor ratios of magnetic Bragg reflections

$$F_M^2(110):F_M^2(111):F_M^2(211)=1:0.855:0.396 \ .$$

On the other hand, in the $(\zeta,0,0)$ scans, broad magnetic scattering was absent, in agreement with the magnetic structure factors listed in Table I $[F_M(200)=F_M(300)=0]$. The same scans were also carried out around both the (210) and (201) reciprocal-lattice points. In the former case, a broad scattering was superimposed on the weak but sharp phonon scattering, while in the latter case, only the strong phonon scattering was detected, in agreement with the structure factors given in Table I. All of these results indicate clearly that the broad scattering,

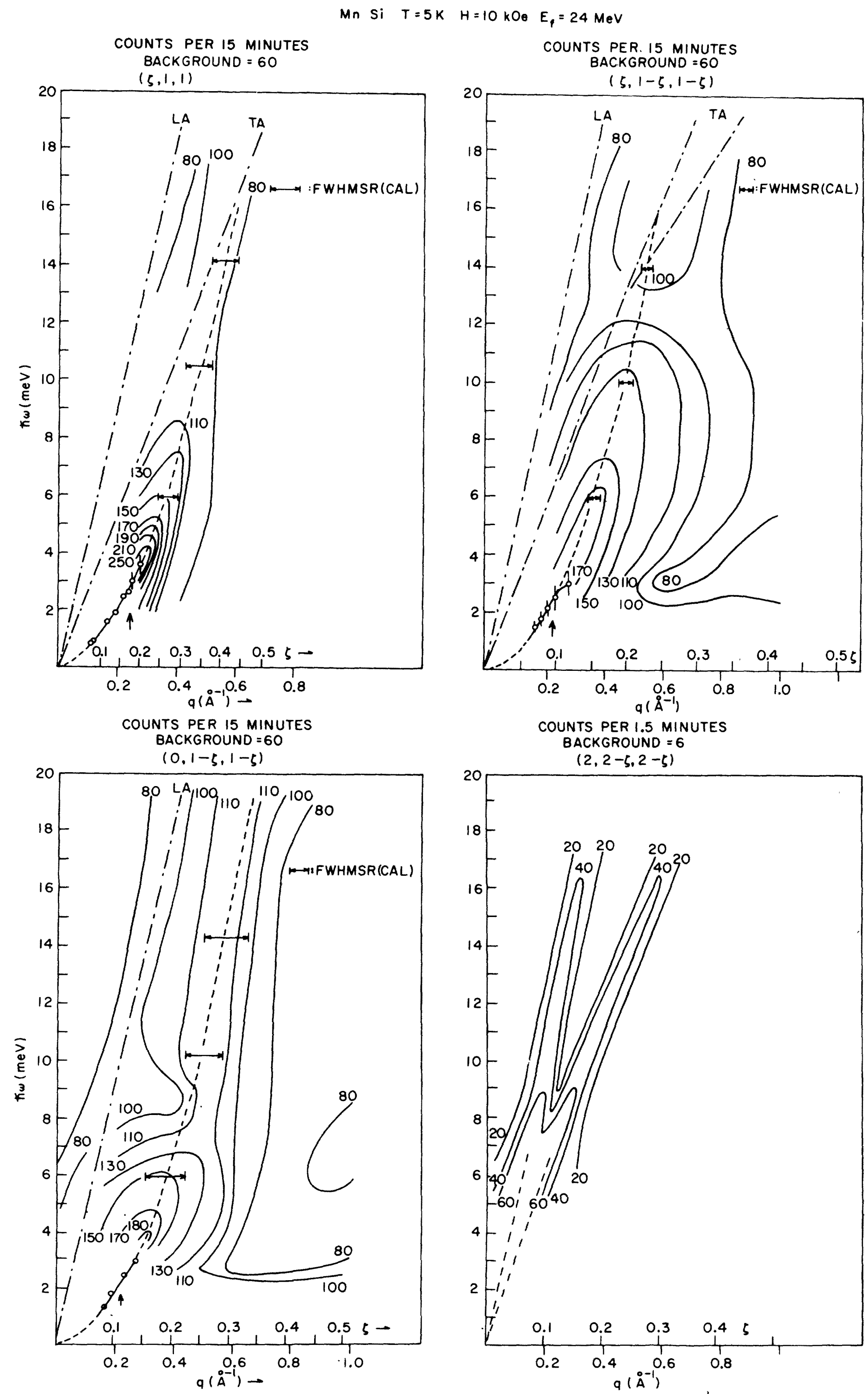

FIG. 8. Contour lines of equal intensity of magnetic scattering at 5 K and 10 kOe measured around (011) reciprocal-lattice point with $E_f = 24$ meV along [100], [111], and [011]. Numbers attached to contour lines are neutron counts per 15 min. Phonon contribution was subtracted. Spin-wave dispersion determined with higher resolution is also included. Horizontal bars with marks FWHMSR are calculated FWHM of magnon groups with infinite lifetime and with quadratic dispersions shown by broken lines. Contour lines of equal intensity of phonon scattering measured along [011] with the same condition as others is also shown for comparison. Monitor time for phonon is $\frac{1}{10}$ of that for magnon.

though independent of temperature, is magnetic in origin.

In order to get the dynamical magnetic response or $\chi(Q,\omega)$ all over the Brillouin zone, complete scans were made in three directions in the (011) Brillouin zone up to an energy transfer of 20 meV and contour lines of equal intensity thus obtained are illustrated together in Fig. 8. Contour lines of acoustical-phonon scattering in the [011] direction are also included for comparison. The FWHM of phonon scattering agrees satisfactorily with the instrumental resolution as shown in Fig. 3. In contour lines of magnetic scattering, the phonon contribution was properly subtracted by connecting smoothly points of equal intensity of magnetic scattering.

In Fig. 8 are also plotted the spin-wave excitation determined with higher resolution of $14.8E_f$ (Fig. 5). Horizontal bars marked FWHMSR indicate the calculated FWHM for the quadratic dispersion relation given by Eq. (5) determined in the spin-wave region. The FWHM is relatively large for the $(\zeta,1,1)$ and $(0,1-\zeta,1-\zeta)$ directions, but it is very small for the $(\zeta,1-\zeta,1-\zeta)$ direction. The former two directions correspond to the poor focusing directions, but the instrumental resolution is still quite narrow compared with the FWHM of the magnetic scattering. The most notable result is that the broad magnetic scattering could be detected up to an energy transfer of 20 meV in three crystallographic directions. The scattering is not isotropic, with the narrowest linewidth in the [100] and the broadest in the [111] direction, but in all three directions the excitation develops along the quadratic dispersion extrapolated from the low-energy region. The excitation is clearly different from the spin-wave mode and would be attributed to quasicollective excitations or spin fluctuations in the Stoner continuum as will be discussed in Sec. III C. The result then provides us with the first example of observation of the spin fluctuation associated with the Stoner excitation in the ferromagnetic state.

C. Excitation in transition region at 5 K

In order to study more carefully how the spin-wave excitation merges into the Stoner continuum, the intrinsic linewidth of the spin-wave excitation in the transition region was estimated by making the resolution correction in the following way. The instrumental resolution or the FWHM, $2\Gamma_{\rm in}$, was calculated by Eq. (4) for the spin-wave excitation with infinite lifetime and the intrinsic linewidth of the excitation was approximately estimated from the observed FWHM,

$$2\Gamma_{\rm ob},\ \text{by}\ 2\Gamma=[(2\Gamma_{\rm ob})^2+(2\Gamma_{\rm in}^2)]^{1/2}$$

The relation is exact for a planar dispersion surface with a Gaussian-type line broadening. The linewidth 2Γ thus obtained from the observation with both of

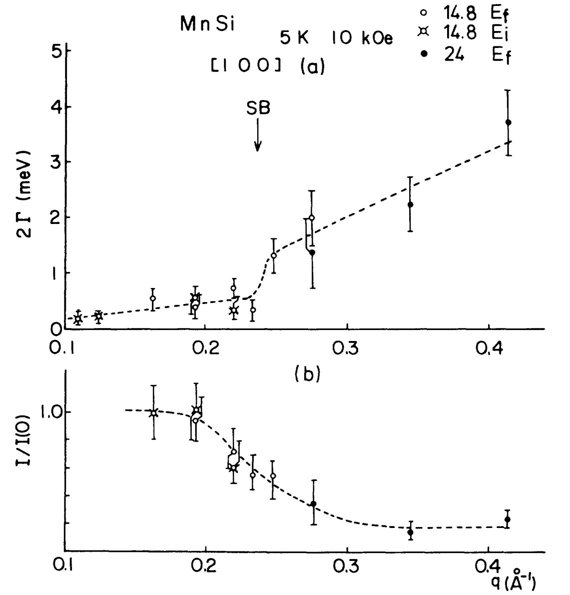

FIG. 9. Intrinsic linewidth (a) as well as integrated intensity (b) of magnons in [100] obtained by resolution correction from data taken at 5 K and 10 kOe with three different conditions of $14.8E_i$, $14.8E_f$, and $24E_f$ plotted against q.

$14.8E_f$ and $24E_f$ scans are plotted against wave vector q in three directions in Fig. 9(a) and Figs. 10(a) and 10(b). The vertical error bars are mainly due to the uncertainty in $2\Gamma_{\rm ob}$. In the [100] direction, the linewidth of the spin-wave excitation increases very little up to a wave vector of $q=0.23$ Å^{-1} ($\zeta=0.17$), where a sudden increase of linewidth occurs as was

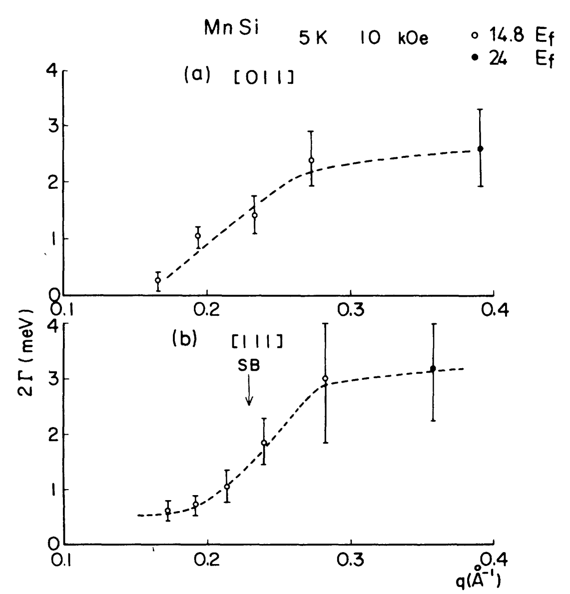

FIG. 10. Intrinsic linewidth of magnons in [011] (a) and in [111] (b) measured at 5 K and 10 kOe plotted against q. Resolution effects were corrected.

seen in Fig. 4. The linewidth then increases further almost linearly with an increase in q.

In Fig. 9(b) the integrated intensities of the magnetic excitation corrected for the instrumental resolution are also plotted against q on a normalized scale. The experimental results obtained with $14.8E_f$ and $24E_f$ were normalized by comparing the intensities of standard phonon peaks measured with both scans. The same procedure could not be applied to normalize the results obtained with higher resolution of $14.8E_f$ and collimations of 20′-20′-20′-40′ with respect to those with $14.8E_f$ condition, because, using the former condition, the standard phonons could not be measured with good precision. The result in Fig. 9(b) indicates that the intensity of spin wave excitations starts to decrease at the wave vector where deviation of the dispersion relation from the quadratic law becomes appreciable (cf. Fig. 5); in other words, the decrease in intensity starts to occur before the spin-wave excitation merges into the Stoner continuum. The intensity decrease seems to saturate above $q = 0.3\,\text{Å}^{-1}$. Note that at 5 K the temperature factor in the scattering cross section [Eq. (3)] varies less that 2% for spin waves with q greater than 0.16, and $I/I(0)$ should then be nearly independent of q if the cross section is described by a one-magnon process.

Such a discontinuous change in the linewidth could not be detected in other directions as seen in Figs. 10(a) and 10(b). The increase in linewidth is rather gradual. In order to see this situation in another way, the magnetic scattering in the transition region was measured over the whole Brillouin zone around (011) with $14.8E_f$ to draw the intensity contours of the scattering. A magnetic field of 10 kOe was always applied in the $[01\bar{1}]$ direction. Contour lines of equal intensity obtained at 5 K are displayed in Figs. 11 and 12(a). The broken line in each figure is the quadratic dispersion relation given in Eq. (5). The contour lines in Fig. 12(a) show most clearly how the spin-wave excitation intersects the Stoner continuum. The Stoner boundary is now marked with an arrow. The boundary exists at an energy transfer of 2.6 ± 0.1 meV for the [100] direction. The boundary is less clear in other directions as seen in Fig. 11. The boundary is around 2.7 meV in the [011] direction and is near 2.4 meV in the [111] direction. In all cases the dispersion has a tendency to bend toward the low-energy side from the quadratic relation just before it touches the Stoner continuum. We can also conclude that the Stoner boundary is almost isotropic and it exists at 2.5 ± 0.2 meV.

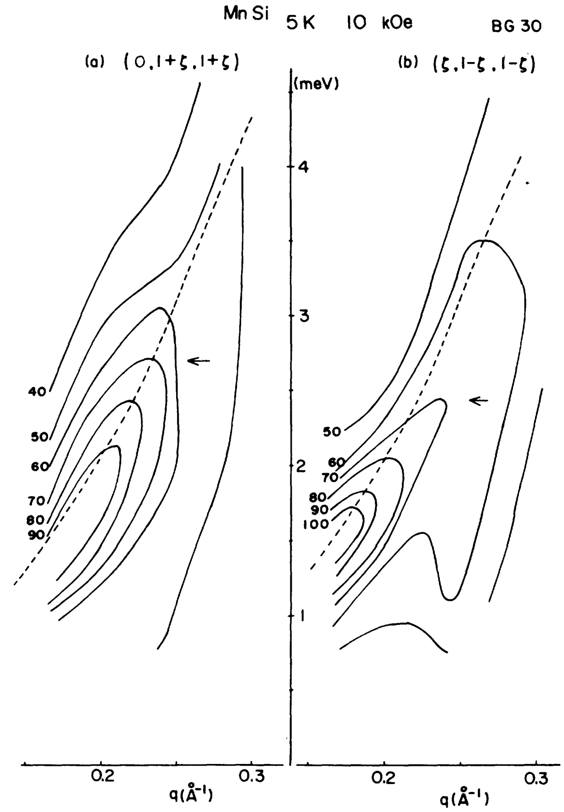

FIG. 11. Contour lines of equal intensity of magnon scattering at 5 K and 10 kOe measured around (011) with $14.8E_f$ along [011] (a) and [111] (b). Numbers attached to contour lines are neutron counts per 15.6 min.

D. Temperature dependence of magnetic excitation

The temperature dependence of spin-wave excitations with small wave vectors has already been discussed in Sec. III A. The investigation of the temperature dependence of spin-wave excitation in the transition region is also quite important because we need to know whether the Stoner boundary varies with temperature. Figure 12(b) and 13 demonstrate contour lines of spin-wave excitation in the [100] direction measured at different temperatures using the same condition as the results in Figs. 11 and 12(a). Near the Stoner boundary, the spin-wave excitation at finite temperatures has a substantially large linewidth, but the intersection of spin waves with the Stoner continuum could still be discriminated even at 24 K with the Stoner boundary shifting to the low-energy and momentum sides. Note that the ratio of the Stoner boundary at 24 K to that at 5 K $E_{SB}(24\text{ K})/E_{SB}(5\text{ K})$ is 0.82, which is close to the ratio of the magnetizations at these temperatures; $M(24\text{ K},10\text{ kOe})/M(5\text{ K},10\text{ kOe}) = 0.82$. Therefore, the Stoner boundary itself seems to decrease in proportion with magnetization. The contour lines at 40 K have a characteristic of the critical scattering; there is no sign of the collective excitation. The critical scattering of this crystal is also of great interest and should be studied with better resolution. This is a problem for future study.

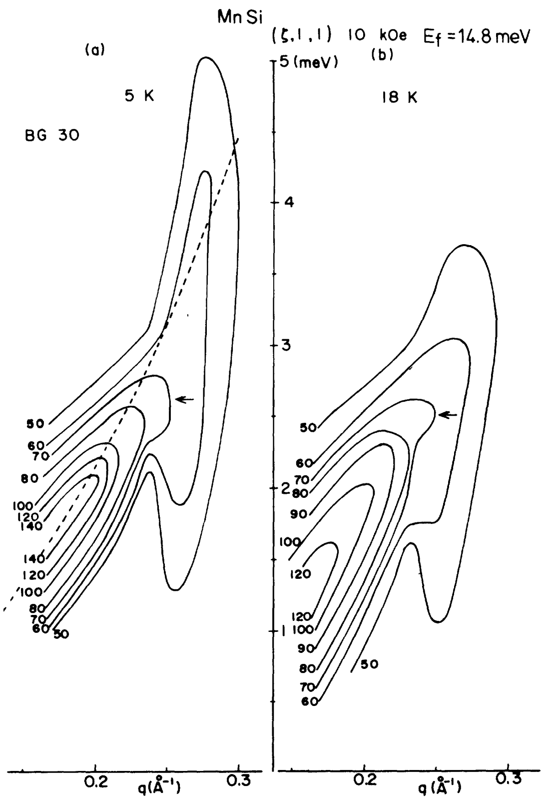

FIG. 12. Contour lines of equal intensity of magnon scattering at 10 kOe measured around (011) with $14.8E_f$ along [100] at 5 K (a) and 18 K (b).

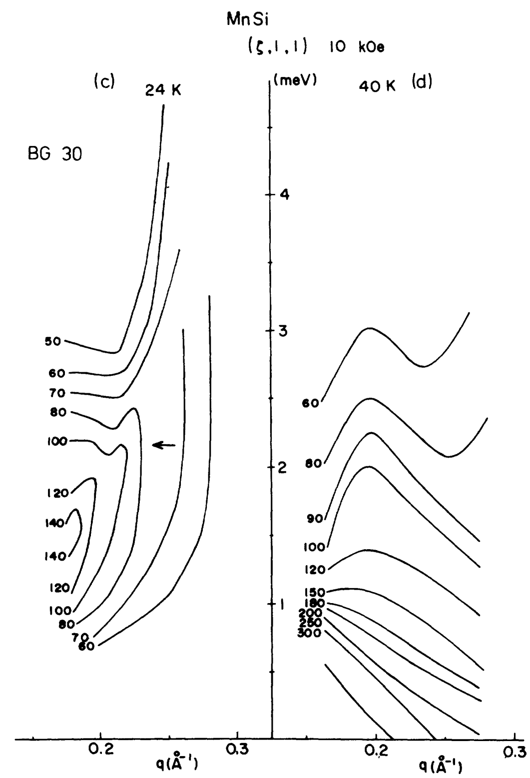

FIG. 13. Contour lines of equal intensity of magnon scattering measured with the same conditions as Fig. 12 at 24 K (c) and 40 K (d).

The temperature dependence of the Stoner excitations was studied without applying a magnetic field, because we have found in Fig. 6(b) that a magnetic field at 10 kOe does not affect the scattering. The crystal was then mounted in a conventional low-temperature cryostat and the scattering in the [011] direction was measured all over the (011) Brillouin zone at three different temperatures of 33, 100, and 270 K. The results at 33 and 270 K are displayed in Figs. 14(a) and 14(b). A broken line in each figure is again the quadratic spin-wave dispersion given in Eq. (5). The contribution from phonon scattering was appropriately subtracted as was done in Fig. 8. Note that the intensity in Fig. 14 cannot directly be compared with that at 5 K (Fig. 8) because of the difference in the crystal environment. The latter experiments were carried out in a superconducting magnet. The most striking result is that contour lines change little even if the temperature is raised to 270 K which is nine times higher than the Néel temperature. A highly damped magnetic excitation still exists with a peak along the quadratic dispersion relation obtained at 5 K. Thus the spin-wave excitation at 0 K is foreseen in the spin fluctuation in the Stoner continuum at high temperatures.

IV. DISCUSSION

A. Comparison with RPA theory for electron gas

The magnetic excitation or the dynamical magnetic response of the itinerant electron ferromagnetic system has been discussed by a number of investigarors.[18,28–31] The most complete study has been performed for the electron-gas system based on a random-phase approximation (RPA). In this model, the dynamical magnetic susceptibility $\chi(Q,\omega)$ is given by

$$\chi(Q,\omega)=\chi_0(Q,\omega)/[1-I\chi_0(Q,\omega)] \ , \tag{6}$$

with $\chi_0(Q,\omega)$ the susceptibility of the noninteracting system and I the intra-atomic interaction. The imaginary part of the susceptibility which is proportional to the neutron-scattering cross section [Eq. (3)] is then given by

$$\mathrm{Im}\chi(Q,\omega)=\frac{\mathrm{Im}\chi_0(Q,\omega)}{[1-I\,\mathrm{Re}\chi_0(Q,\omega)]^2+[I\,\mathrm{Im}\chi_0(Q,\omega)]^2} \ . \tag{7}$$

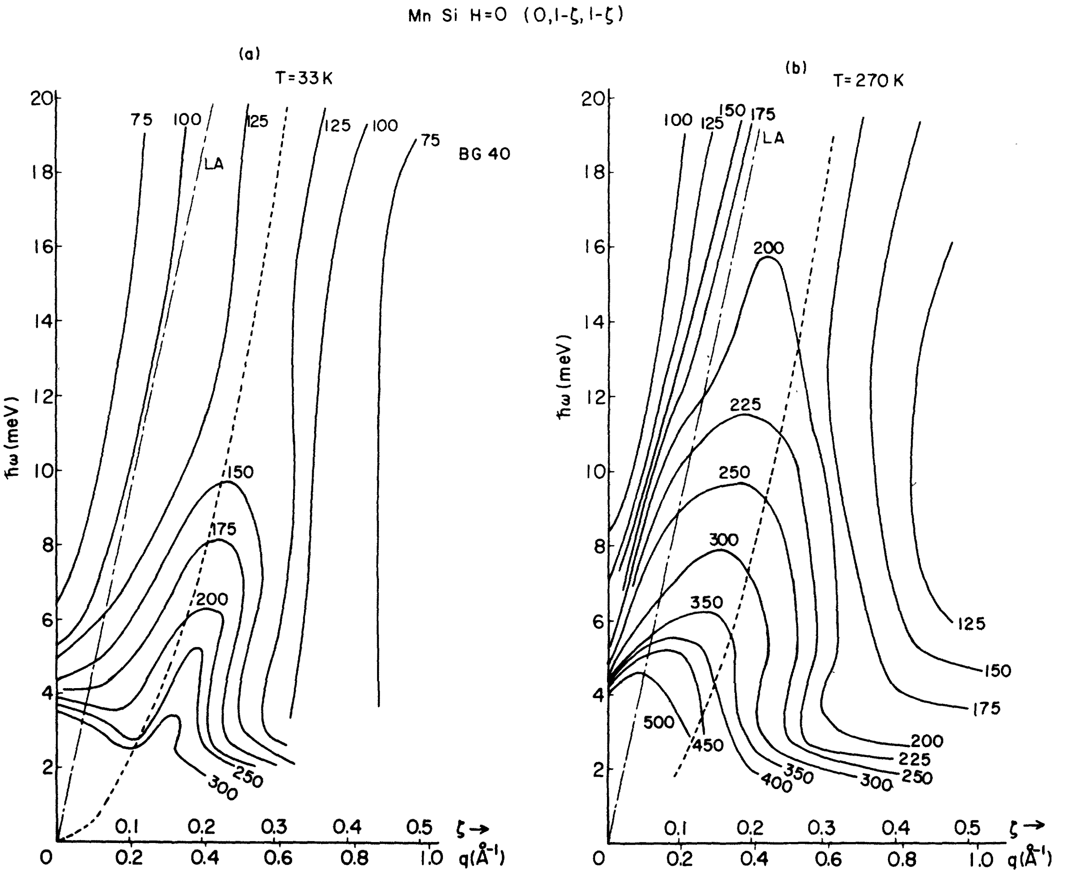

FIG. 14. Contour lines of equal intensity of magnetic scattering measured along [011] in zero field with $24E_f$ at $T=33$ K (a) and 270 K (b). Numbers attached to contour lines are neutron counts per 15 min.

$\chi_0(Q,\omega)$ can be calculated analytically for the electron gas and the results show that two types of excitation exist in the ferromagnetic system. One is the excitation observed in the region I in Fig. 2 where $\mathrm{Im}\chi_0(Q,\omega)$ is zero. Equation (7) then reduces to a δ function and a well-defined spin-wave excitation appears when

$$1-I\,\mathrm{Re}\chi_0(Q,\omega)=0 \ . \tag{8}$$

This relation gives the spin-wave dispersion which is traced by a solid line in Fig. 2. For small wave vector q, the dispersion is quadratic in q with an exchange stiffness constant D given by

$$D=\frac{\hbar^2 In}{2m\Delta}\left[1-\frac{4}{5n\Delta}(\epsilon_F^+ n^+ - \epsilon_F^- n^-)\right] \tag{9}$$

for the electron gas with energy splitting Δ. ϵ_F^+ (ϵ_F^-) and n^+ (n^-) are the Fermi energy and electron number of the up-spin band (down-spin band), respectively, and $n=n^+ + n^-$. Δ is self-consistently determined by a relation

$$\Delta = I(n^+ - n^-) = Im/\mu_B \ , \tag{10}$$

where m is the ferromagnetic moment of the system. When $\Delta/\epsilon_F^+ = \zeta << 1$, which is the case for the weak itinerant-electron ferromagnetism, D and m being expressed as

$$D \approx (\hbar^2/2m)\tfrac{1}{12}\zeta/(1-\tfrac{1}{4}\zeta) \ , \tag{11}$$

$$m/n \approx \tfrac{3}{4}\zeta\mu_B \ . \tag{12}$$

D is therefore approximately proportional to the magnetic moment.

There is another region marked as II in Fig. 2 where $\mathrm{Im}\chi_0(Q,\omega)$ has nonzero value. This is the region where the excitation of an itinerant electron from one spin band to another (the Stoner excitation) can occur. A simple RPA calculation shows that the spin wave dispersion approaches the Stoner continuum so as to intersect the Stoner boundary tangentially as schematically shown in Fig. 2. The intensity of neutron spin-wave scattering decreases gradually on approaching the boundary but without line broadening.

The linewidth increases rapidly once the dispersion merges into the Stoner continuum.

$\mathrm{Im}\chi(Q,\omega)$ in this region was calculated for the electron gas by Seki and Tachiki[32] and contour lines of $\mathrm{Im}\chi(Q,\omega)$ for $\zeta=0.3$ are presented in Fig. 15 to compare with the observation (Fig. 8). The parameter $\zeta=0.3$ corresponds to the system with a total of two d electrons and a magnetic moment of 0.45 μ_B. The energy spectra of magnetic scattering from the electron gas were calculated for constant momentum transfer by convoluting a simple resolution function $R(\Delta\omega)=R_0\exp-(\Delta\omega)^2/\Gamma_0^2$ with $\mathrm{Im}\chi(Q,\omega)$ in Fig. 15. Variations of the linewidth Γ (FWHM) as well as the peak intensity I_p of the spectra along the peak ridge are plotted against momentum transfers q/k_F in Fig. 16 by solid lines. Chain lines are linewidth corrected for resolution by the method discussed at the beginning of Sec. III and integrated intensity calculated by $I_p\Gamma/\Gamma(0)$, respectively. $2\Gamma(0)$ is the apparent linewidth (FWHM) in the spin-wave region $[\Gamma(0)=\Gamma_0(\ln 2)^{1/2}]$. These chain lines can be compared with Figs. 9(a) and 9(b). The results indicate clearly that the linewidth starts to increase at the Stoner boundary but the integrated intensity decreases gradually on approaching the boundary and, instead of

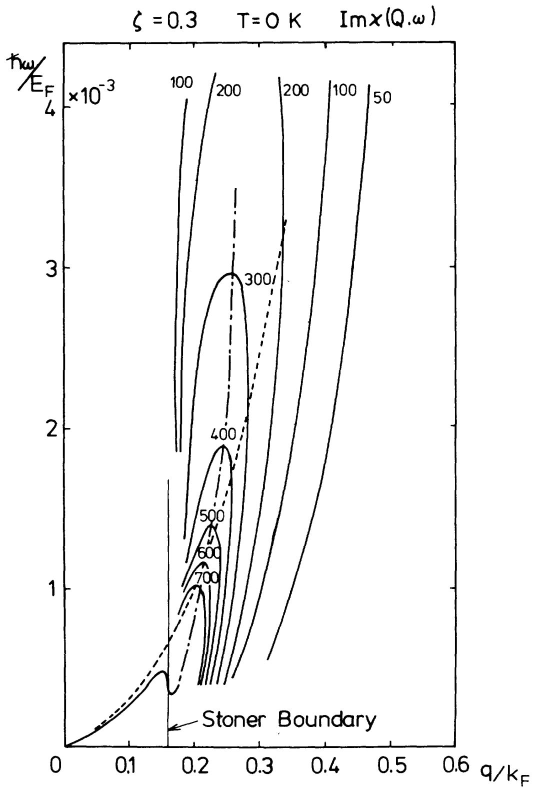

FIG. 15. Magnetic excitation at 0 K in the ferromagnetic electron gas with $\zeta=0.3$ calculated based on RPA. Excitation in the Stoner continuum is displayed as contour lines of equal intensity of $\mathrm{Im}\chi(Q,\omega)$.

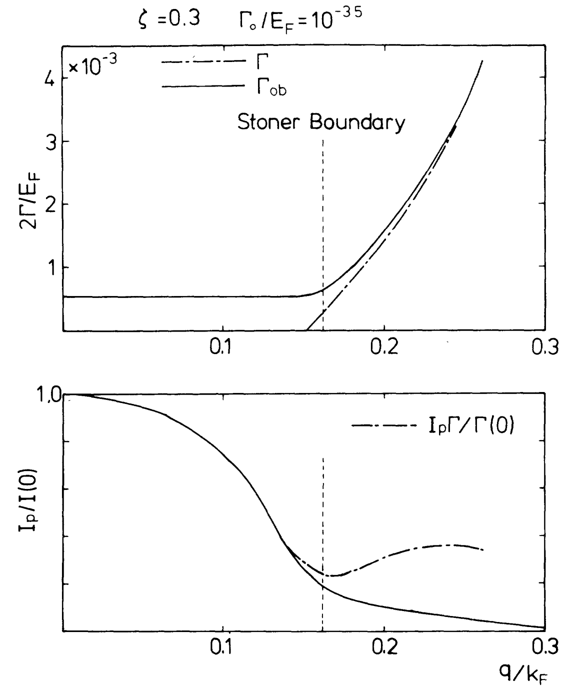

FIG. 16. Variations of apparent linewidth Γ (a) and peak intensity I_p (b) of energy spectra along peak ridge calculated by convoluting a resolution function $R(\Delta\omega)=R_0\exp(-\Delta\omega^2/\Gamma_0^2)$ with $\mathrm{Im}\chi(Q,\omega)$ in Fig. 15 plotted against momentum transfers q/q_F. Intrinsic linewidth evaluated by Eq. (4) as well as integrated intensity calculated by $I_p\Gamma/\Gamma(0)$ are also plotted by chain lines to compare with Fig. 9.

disappearing there, it is smoothly connected with the excitation in the Stoner region through the boundary. Note that the pronounced decrease of the integrated intensity in the spin-wave region is the result of the decreasing energy difference between the Stoner boundary and the spin-wave excitations.

When the temperature is raised, the band splitting Δ or ζ decreases in proportion with the magnetization [Eq. (10)] which in turn reduces the exchange stiffness constant [Eq. (11)] as well as the energy E_{SB} of the Stoner boundary. The calculation of the magnetic excitation at a finite temperature in the Stoner region has not yet been performed, but judging from the results at 0 K for different ζ and $\zeta=0$, we may safely say that the excitations remain qualitatively unchanged as paramagnons[28] even in the paramagnetic state.

This simple RPA picture of magnetic excitations in the electron gas explains qualitatively quite well the fundamental features of the magnetic excitations in MnSi; the spin-wave excitations with infinite lifetime exist in a small wave-vector q region (Fig. 4), the dispersion is quadratic in q but a deviation from this relation occurs near the Stoner boundary (Fig. 5), the intensity of the spin-wave scattering decreases gradually [Fig. 9(b)], while the increase of the linewidth is small up to the boundary [Fig. 9(a)]. $\mathrm{Im}\chi(Q,\omega)$ of MnSi at 0 K is qualitatively the same as contour lines of scattering intensity displayed in Fig. 8, because the temperature factor $1/[1-\exp(-\hbar\omega/kT)]$ in Eq. (3) is practically 1 for the energy transfers greater than 2 meV at 5 K. The contour lines of $\mathrm{Im}\chi(Q,\omega)$ in Fig. 15(a) compare well with the observation. The parameter ζ used in the calculation would be the maximum value for MnSi because the number of d electrons in MnSi may be between 6 and 2. If $\zeta=0.3$, the electron gas model gives the energy of Stoner boundary as about $5\times10^{-4}E_F^{+}$. The result suggests that the observed Stoner boundary of 3 meV can be expected for the weak itinerant ferromagnet with a Fermi energy of the order of 1 eV. The electron-gas model, however, usually gives too small a value for the exchange stiffness constant and for the detailed comparison of RPA theory with the observation, the calculation based on the actual band is required.

With elevating temperature, the exchange stiffness constant as well as the Stoner boundary actually decrease in proportion with the magnetization [Figs. 7, 12(b), and 13]. $\mathrm{Im}\chi(Q,\omega)$ above 30 K was estimated from Fig. 14 by correcting for the temperature factor and magnetic form factor $|F(Q)|^2$. The results at three different temperatures are illustrated in Fig. 17. This figure now shows clearly the temperature variation of $\mathrm{Im}\chi(Q,\omega)$. The quasicollective excitation which exists around the energy transfer of 3 meV at 33 K ($T/T_N=1.1$) shifts to higher energy at higher temperatures. The quasicollective excitation would correspond to the excitation in the short-range order which is not taken into account in the RPA model. Except for this, the fundamental features of the excitation are not varied with temperature as predicted in the theory.

From these similarities between the observation and the electron-gas model, we may conclude that MnSi is an itinerant electron system with a Stoner boundary of less than 3 meV. When the temperature is raised, the Stoner-type excitation takes place substantially, together with the spin-wave excitation. Therefore, the temperature dependence of the magnetization should be governed by both types of excitation as was observed experimentally.

There are also many aspects which cannot be explained by the simple RPA theory. The most important one is that the maximum ridge of contour lines of the magnetic excitation in the Stoner region coincides with the quadratic dispersion of the spin wave. In the case of RPA, the extrapolation of the spin-wave dispersion is always below the maximum ridge for high-energy transfers as shown by a broken line in Fig. 15. The behavior is closer to the dynamical

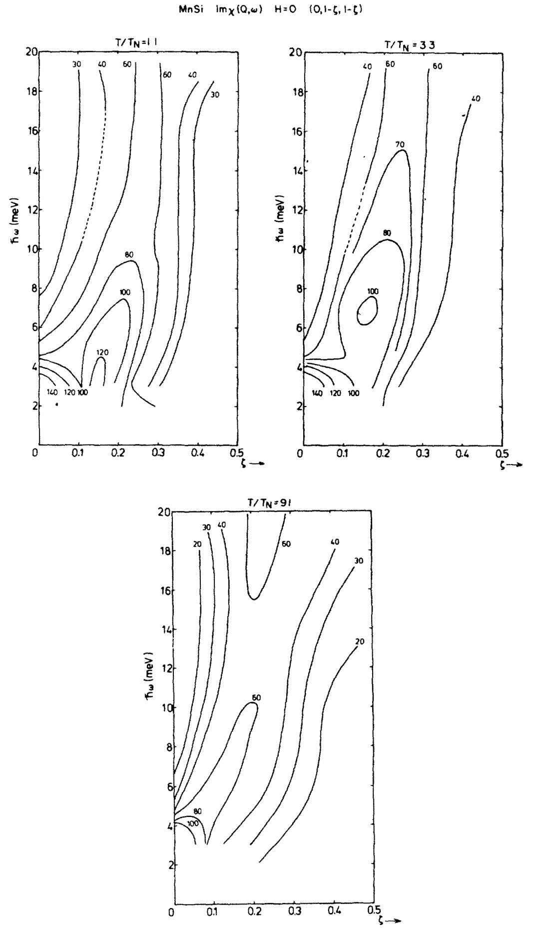

FIG. 17. $\mathrm{Im}\chi(Q,\omega)$ of MnSi in the [011] direction above T_N estimated from low-resolution neutron-scattering cross section (Fig. 14) after background was subtracted. Resolution correction was not performed.

response of the s-d system in the nonadiabatic region.[33] In this case a highly damped magnetic excitation also appears in the Stoner continuum of the conduction electron, but with the same dispersion relation as that in the adiabatic retion (for small wave vectors). Therefore the RPA theory would be improved if the correlation effect is more properly taken into account.[31] Note that the s-d model itself cannot be applied to this system because this model predicts that the magnetic excitations in the Stoner region should disappear above the Curie temperature, which is not the case.

B. Low-energy magnetic excitation; comparison with the Moriya-Kawabata spin-fluctuation theory

As stated in Sec. I, Moriya and his co-workers have developed a new theory to improve the RPA theory by taking into account the transverse spin fluctuation in a self-consistent way and have shown that the long-wave spin fluctuation plays the most important role in determining the magnetic properties of the weak itinerant ferromagnet.[21] According to this theory, the dynamical susceptibility $\chi(Q,\omega)$ is given by

$$\chi(Q,\omega)=\frac{\chi_0(Q,\omega)}{1-I\chi_0(Q,\omega)+\lambda(Q,\omega)} \quad . \tag{13}$$

An additional term $\lambda(Q,\omega)$ to RPA contributes to produce a $T^{3/2}$ temperature dependence of magnetization at low temperatures[34] and the Curie-Weiss law for $\chi(0,0)$ above the Curie temperature.[21] In other words, this term makes the behavior of long-wavelength spin fluctuations in the itinerant electron system like that in the Heisenberg system. Actually the spin-wave excitation with small q resembles that in the Heisenberg system as discussed in Sec. III A. Furthermore, the low-energy excitation below 3 meV seems to make a main contribution to the temperature dependence of the magnetic response above the Curie temperature T_C. For example, the static susceptibility $\chi(0)$ above T_C which obeys the Curie-Weiss law can be estimated from the dynamical susceptibility $\chi(Q,\omega)$ using the Kramers-Kronig relation

$$\begin{aligned}\chi(0)&=\chi(Q=0,\omega=0)\\&=\frac{2}{\pi}\int_0^\infty\frac{\mathrm{Im}\chi(0,\omega')}{\omega'}\,d\omega' \quad .\end{aligned} \tag{14}$$

Figures 17(a), 17(b), and 17(c) indicate that $\mathrm{Im}\chi(0,\omega')$ is almost the same for three temperatures, suggesting the main contribution to $\chi(0)$ is the excitation below 3 meV which is developed around the center of the reciprocal lattice like the critical scattering. This excitation contributes to many physical properties such as the electrical resistivity, specific heat, NMR, etc. in a manner somewhat similar to the Heisenberg system. In order to make a quantitative comparison with the MK theory, more-accurate measurements of the low-energy excitation both below and above T_C as well as the theory based on the actual band are highly required.

V. CONCLUSIONS

Neutron-scattering experiments have revealed that two types of magnetic excitation exist in MnSi. One is the spin-wave excitation with infinite lifetime which follows a quadratic relation below 2 meV. The excitation is renormalized with temperature and it collapses into the critical scattering above the critical temperature. The behavior is quite similar to the spin dynamics in the Heisenberg system. Another is the broad excitation extending over the whole Brillouin zone and we assign it as the excitation in the Stoner continuum. The excitation develops along the quadratic dispersion relation extrapolated from the spin-wave excitation and the excitation changes little with temperature up to $T/T_N=10$. The qualitative features of the excitation are well described by the RPA theory for the electron gas with a small band splitting. Therefore the magnetic excitation found in MnSi would demonstrate a typical characteristic of the dynamical behavior in the weak itinerant ferromagnet. Temperature dependence of low-energy excitation would be consistent with the MK theory though we need further detailed studies to make the quantitative comparison. Some disagreements between the observation and the RPA theory were found and the development of the theory to reconcile them is now highly desired.

ACKNOWLEDGMENTS

We have profited greatly from discussion with M. Tachiki, T. Moriya, T. Kasuya, M. Blume, and R. D. Lowde. A computer calculation $\chi(Q,\omega)$ was made by S. Seki and the sample was prepared by Y. Miura at Institute for Iron Steel and Other Metals to whom authors acknowledge gratefully. One of the authors (Y.I.) thanks all colleagues at Brookhaven National Laboratory for kind hospitality he received during his stay there.

---

*Permanent address: Physics Dept., Tohoku University, Sendai; now returned.

†Work supported by U. S. Energy Research and Development Administration under Contract No. EY-76-C-02-0016.

[1]H. J. Williams, J. H. Wernick, R. C. Sherwood, and G. K. Wertheim, J. Appl. Phys. 37, 1256 (1966).

[2]D. Shinoda and S. Asanabe, J. Phys. Soc. Jpn. 21, 555 (1966).

[3]J. H. Wernick, G. K. Wertheim, and R. C. Sherwood, Mat. Res. Bull. 7, 1431 (1971).

[4]L. M. Levinson, G. H. Lander, and M. O. Steinitz, AIP Conf. Proc. 10, 1138 (1972).

[5]S. Asanabe, D. Shinoda, and Y. Sasaki, Phys. Rev 134, A774 (1964).

[6]H. Watanabe, H. Yamamoto, and K. Ito, J. Phys. Soc. Jpn. 18, 995 (1965).

[7]V. Jaccarino, G. K. Wertheim, and J. H. Wernick, Phys. Rev. 160, 476 (1967).

[8]S. Ogawa, Res. Rept. Electrotechnical Lab. No. 735 (1972) (unpublished).

[9]Y. Ishikawa, K. Tajima, D. Bloch, and M. Roth, Solid State Commun. 19, 525 (1976).

[10]D. Bloch, J. Voiron, V. Jaccarino, and J. H. Wernick, Phys. Lett. A 51, 259 (1975).
[11]H. Yasuoka (private communication).
[12]E. P. Wohlfarth, J. Appl. Phys. 39, 1061 (1968).
[13]E. Fawcett, J P Maita, and J. H. Wernick, Intern. J. Magn. 1, 29 (1970). In this paper an error was made in presenting the specific-heat data for MnSi: in Figs. 2 and 3, the scale for specific heat values is too large by a factor of 10. The resultant estimates of the magnetic entropy S_m and the magnetic Grüneisen parameter γ_m are also wrong by a factor of 10. The correct values are $S_m = 0.092$ cal $\mathrm{K^{-1} mol^{-1}}$ in zero field and $S_m = 0.089$ cal $\mathrm{K^{-1} mol^{-1}}$ in a field of 9 kOe, and $\gamma_m = -46$. Thus the logarithmic derivative of the magnetic interaction parameter J is $\partial \ln J(V)/\partial \ln V = +46$, instead of $+4.6$, whereas the value of the electronic Grüneisen parameter is correctly given as $\gamma_e = -10$. [E. Fawcett, (private communication).]
[14]S. Kusaka, K. Yamamoto T. Komatsubara, and Y. Ishikawa, Solid State Commun. 20, 927 (1976).
[15]Y. Ishikawa, T. Komatsubara, and D. Bloch, Physica (Utr.) 86-88B, 401 (1977).
[16]Y. Ishikawa, Proceedings of the International Conference on Itinerant Magnetism, 1977 (unpublished).
[17]C. Herring, *Magnetism,* edited by G. T. Rado and H. Suhl (Academic, New York, 1967), Vol IV.
[18]R. D. Lowde and C. G. Windsor, Adv. Phys. 19, 813 (1970).
[19]H. A. Mook, R. M. Nicklow, E. D. Thompson, and M. K. Wilkinson, J. Appl. Phys. 39, 1450 (1969).
[20]H. A. Mook and R. M. Nicklow, Phys. Rev. B 7, 336 (1973).
[21]T. Moriya and A. Kawabata, J. Phys. Soc. Jpn. 34, 639 (1973); see also, T. Moriya, Physica (Utr.) B 91, 235 (1977).
[22]M. Date, K. Okuda, and K. Kadowaki, J. Phys. Soc. Jpn. 42, 1555 (1977).
[23]L. Pauling and A. M. Soldate, Acta. Crystallogr. 1, 212 (1948).
[24]W. Marshall and S. W. Lovesey, *Theory of Thermal Neutron Scattering* (Oxford U. P., London, 1971).
[25]H. Patterson, G. Shirane, and R. A. Cowley, Brookhaven National Lab. Research Memo G-29 (1976) (unpublished).
[26]M. J. Cooper and R. Nathans, Acta Crystallogr. 28, 357 (1967).
[27]N. J. Chesser and J. D. Axe, Acta Crystallogr. A 29, 160 (1973).
[28]T. Izuyama, D. J. Kim, and R. Kubo, J. Phys. Soc. Jpn. 18, 1025 (1963).
[29]S. Doniach, Proc. Phys. Soc. Lond. 91, 86 (1967).
[30]G. Barnea and G. Horwitz, J. Phys. C 6, 738 (1973).
[31]S. H. Liu, Phys. Rev. B 13, 3962 (1976).
[32]S. Seki, M. Tachiki, and Y. Ishikawa (unpublished).
[33]Y. Nagaoka, Prog. Theor. Phys. 28, 1033 (1962).
[34]T. Moriya and A. Kawabata, J. Phys. Soc. Jpn. 35, 669 (1973).